Effect of Perturbation on the Whipping Motion in Electrospinning

J. P. Yang, Y. C. Zeng, Z. G. Pei, X. H. Wang

College of Textiles, Donghua University, Songjiang, Shanghai 201620, People's Republic of China

Received 29 April 2009; accepted 18 July 2009
DOI 10.1002/app.31140
Published online 15 October 2009 in Wiley InterScience (www.interscience.wiley.com).

ABSTRACT: Recent studies have demonstrated that the essential electrospinning mechanism is a rapidly whipping jet in an electric field. Perturbation growth is responsible for the observed whipping motion in electrospinning. In this study, we focused on the effect of perturbation on the whipping motion in electrospinning. Experimental and modeling studies were performed. Experimental observations by electrospinning under normal and vacuum conditions showed that perturbations caused by the ambient air influenced the whipping motion and fiber diameter. Modeling predictions also showed the effect of the initial perturbation on the whipping instability, and qualitative trends in the model predictions were in accordance with the experimental investigation. © 2009 Wiley Periodicals, Inc. J Appl Polym Sci 115: 2508–2513, 2010

Key words: drawing; extrusion; fibers; modeling; processing

INTRODUCTION

The physical mechanism of the electrospinning process has been explained and described by several researchers.[1–7] It has been shown that the longitudinal stress caused by the electric field acting on the charge carried by the jet stabilizes the straight jet for some distance. Then, a lateral perturbation grows in response to the repulsive forces between the adjacent elements of charge carried by the jet. The perturbation grows to become observed as whipping motion, which is the key physical element of the electrospinning process responsible for the enormously strong stretching and the formation of nanofibers. The authors of these works have explained the reasons for the observed bending instability of jets in electrospinning. Lateral perturbation seems to play an important role in the whipping instability, whereas no researchers have explored the relationship between perturbations and the whipping motion.

In this study, we adopted the electrospinning model described in our previous article[8] to predict the effect of perturbation on the whipping instability and to compare the prediction results to experimental results on poly(ethylene oxide) (PEO) and poly (vinyl alcohol) (PVA). To study the effect of perturbation on the whipping motion experimentally, we performed electrospinning experiments under normal and vacuum conditions and investigated the resulting fiber diameters under different conditions. Here, we focused on the perturbation caused by ambient air during the electrospinning process. In fact, in the vacuum condition, the rare air led to a weaker perturbation in the electrospinning process.

EXPERIMENTAL

Experimental procedure

PEO and PVA were chosen for the electrospinning experiments. PEO (number-average molecular weight = 1,000,000) was dissolved in deionized water to make a 5% (g/mL) solution for the experiments. The viscosity of the 5% PEO solution was 695 mPa s. PVA (number-average molecular weight = 10,000) was dissolved in deionized water to make an 8% (g/mL) solution for the experiments. The viscosity of the 8% PVA solution was 355 mPa s.

The experimental setup is shown in Figure 1. In this setup, the syringe needle and the collector of the electrospinning apparatus were installed inside a 40×40 cm^2 chamber. A 20×20 cm^2 lid was in one of the faces of the chamber. The solution was forced through the syringe needle via a Cole-Parmer syringe pump (Cole-Parmer Instrument Co., Vernon Hills, IL). When the solution was electrospun under vacuum conditions, the chamber was sealed and vacuumed via a vacuum pump before electrospinning. Although the solution was electrospun under

Correspondence to: Y. C. Zeng (yongchun@dhu.edu.cn).
Contract grant sponsor: Foundation for the Author of National Excellent Doctoral Dissertation of the People's Republic of China; contract grant number: 2007B54.
Contract grant sponsor: The National Natural Science Foundation of China; contract grant number: 10972052.

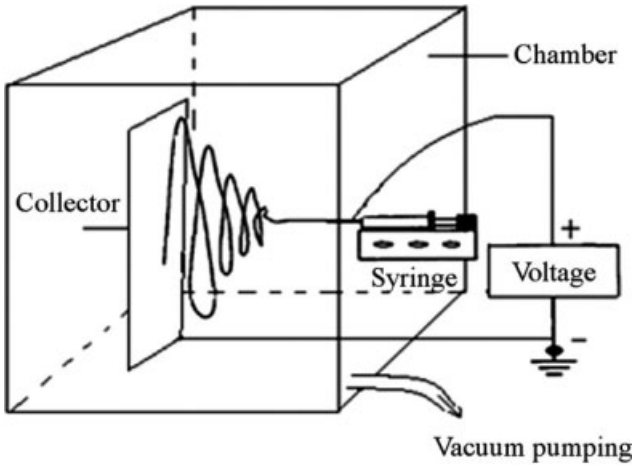

Figure 1 Schematic diagram of the electrospinning *in vacuo*.

normal conditions, the lid was taken away, and the electrospinning was performed at atmospheric pressure. In the electrospinning experiments, the processing parameters were set as applied voltage (V) = 15 kV, solution flow rate (Q) = 0.5 mL/h, tip-to-collector distance (H) = 20 cm, needle inner diameter (d) = 1 mm, and period for collecting = 10 min.

The collected electrospun fibers were observed by scanning electron microscopy (SEM; DXS-10ACKT, Shanghai, China). Image processing and the analysis of the fiber diameter were performed with Image J image analysis software.

Characterizing whipping motion is not a simple task, either by experimental or theoretical methods. Recently, Yang et al.[9] used the initial angle of the looping envelop (Ω), the bending frequency of the first few loops (ω), and the helical pitch to characterize whipping instability. However, the measurements of these parameters were very difficult. In this analysis, the effect of perturbation on the whipping motion was evaluated by an indirect parameter: the area of the collected mat (S). S was defined as the deposited area of the fibers on the collector. An image of the collected mat was obtained with a scanner. Image processing and the measurement of S was performed with Image J software. As shown in Figure 2, the fiber mat collected on the collector covered an almost round area. When the period of fiber collecting was constant, say, 10 min, a larger S indicated a stronger whipping motion.

Experimental results

The electrospinning experiments were performed under normal and vacuum conditions, with the processing parameters unvaried. To evaluate the effects of different vacuums on the whipping motion, two vacuum conditions, −0.02 and −0.03 MPa, were used. In these experiments, the higher vacuum was difficult to obtain because of the low strength of the vacuum chamber.

The resulting diameters and the S values of the PEO fibers spun under normal and vacuum conditions are shown in Table I. Figure 3 shows the SEM micrographs of the fibers that were electrospun from PEO. The results of the experiments on PVA are shown in Table II and Figure 4. As shown by these results, the fibers obtained under vacuum conditions were coarser than those obtained under normal conditions, and the higher vacuum of −0.03 MPa gave the largest fiber diameter. The fiber diameter range (i.e., the range of the maximum and minimum fiber diameters) under normal conditions was a bit smaller than those under vacuum conditions. For the PEO fibers, the maximum diameter spun under normal conditions was 143 nm, whereas the maximum diameters spun under −0.02 and −0.03 MPa were 180 and 228 nm, respectively. For the PVA fibers, the maximum diameter spun under normal conditions was 134 nm, whereas the maximum diameters spun under −0.02 and −0.03 MPa were 173 and 197 nm, respectively. With regard to S, the values obtained under vacuum conditions were smaller than that obtained under normal conditions, and the

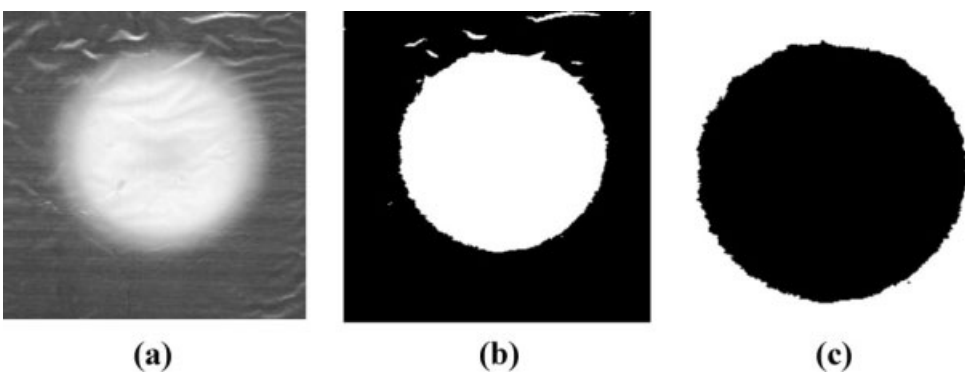

Figure 2 Measurement of *S:* (a) image obtained by a scanner, (b) image processed by Image J software, and (c) final processed image.

TABLE I
PEO Fiber Diameters and *S* Values for Fibers Spun Under Normal and Vacuum Conditions

Condition	Normal	−0.02 MPa	−0.03 MPa
S (cm^2)	51.4	40.5	35.1
Average fiber diameter (nm)	120	146	164
Fiber diameter range (nm)	85	91	97

Processing parameters: solution concentration = 5%, V = 15 kV, Q = 0.5 mL/h, H = 20 cm, and d = 1 mm.

TABLE II
PVA Fiber Diameters and *S* Values of Fibers Spun Under Normal and Vacuum Conditions

Condition	Normal	−0.02 MPa	−0.03 MPa
S (cm^2)	48.1	36.6	31.7
Average fiber diameter (nm)	116	131	140
Fiber diameter range (nm)	67	75	76

Processing parameters: solution concentration = 8%, V = 15 kV, Q = 0.5 mL/h, H = 20 cm, and d = 1 mm.

higher vacuum of −0.03 MPa led to the smallest S. As mentioned previously, a larger S indicates a stronger whipping motion. The smaller S obtained under vacuum conditions may have been due the rare air in the vacuum. The rare air gave rise to a weaker perturbation in the electrospinning process and, therefore, suppressed the whipping motion. The weaker whipping motion in a vacuum led to smaller stretching during electrospinning, which resulted in coarser fibers. As one can see, a weaker perturbation in the process caused slightly weaker whipping and a slightly larger fiber diameter. Although the differences were small, the directions of change were as expected.

MODELING STUDY

The linear and nonlinear models of the dynamics of bending instability in electrospinning were developed by Rutledge and coworkers,[1–4] and Reneker and Yarin and coworkers[5–7] However, the relationship between the amplitude of the whipping instability and the final fiber diameter was not explored in these articles. Recently, Fridrikh et al.[10] modeled the nonlinear whipping behavior of an electrospinning jet. Their model predicts the amplitude of the whipping instability causing the formation of nanofibers to saturate and the jet to reach a terminal diameter controlled by the surface tension, surface charge repulsion, and solvent evaporation. In their model, one can determine the terminal jet radius by balancing the charge repulsion and the surface tensions.

In our previous study,[9] the whipping motion of electrospinning was simulated. In the this study, we adopted a developed mathematical model to study the effect of perturbation on the whipping motion and final fiber diameter.

The electrospun jet (fiber) was modeled as a bead-viscoelastic element chain. The total number of beads (N) increased over time as new electrically charged beads were inserted at the top to represent the flow of the solution into the jet. The three-dimensional equation of the dynamics of the electrospun jets is

$$m\frac{d^2r_i}{dt^2} = F_{Ci} + F_{Ei} + F_{vei} + F_{Bi} \quad (1)$$

where m is the mass of bead i, $r_i = \mathbf{i}x_i + \mathbf{j}y_i + \mathbf{k}z_i$ is the position of bead i, and **i, j,** and **k** are the unit vectors along the x, y, and z axes, respectively. F_{Ci} is the net Coulomb force acting on bead i from all of the other beads and is expressed as

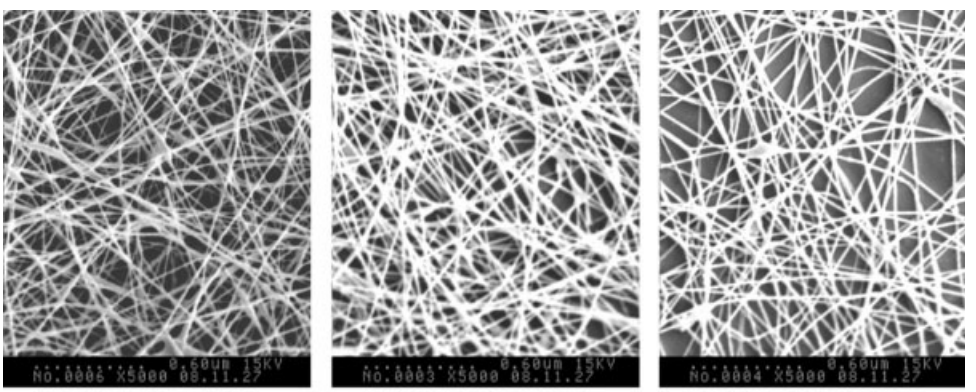

Figure 3 SEM images of the PEO fibers electrospun under (a) normal conditions, (b) at −0.02 MPa, and (c) at −0.03 MPa (processing parameters: solution concentration = 5%, V = 15 kV, Q = 0.5 mL/h, H = 20 cm, and d = 1 mm).

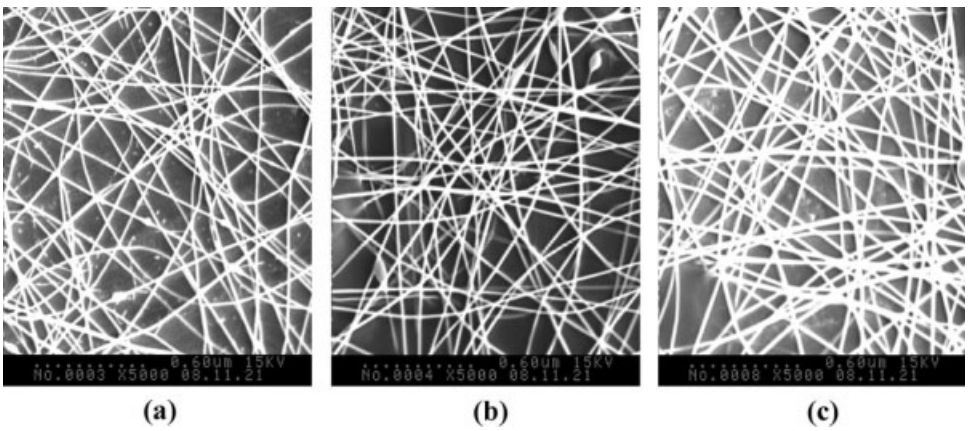

Figure 4 SEM images of the PVA fibers electrospun under (a) normal conditions, (b) at −0.02 MPa, and (c) at −0.03 MPa (processing parameters: solution concentration = 8%, V = 15 kV, Q = 0.5 mL/h, H = 20 cm, and d = 1 mm).

$$F_{Ci} = \sum_{\substack{j=1 \\ j\neq i}}^{N} \frac{e^2}{R_{ij}^2}\left[\frac{r_i - r_j}{R_{ij}}\right] \tag{2}$$

where e is the charge each bead possesses and R_{ij} is the distance between bead i and bead j. F_{Ei} is the electric force imposed on bead i by the electric field and is expressed as

$$F_{Ei} = -e\frac{V_0}{h}\mathbf{k} \tag{3}$$

where V_0 is the applied voltage and h is the distance from the spinneret to the collector. F_{vei} is the net viscoelastic force acting on bead i and is expressed as

$$F_{vei} = \frac{\pi d_{i,i+1}^2}{4}\sigma_{i,i+1}\left[\frac{r_{i+1} - r_i}{l_{i,i+1}}\right] - \frac{\pi d_{i-1,i}^2}{4}\sigma_{i-1,i}\left[\frac{r_i - r_{i-1}}{l_{i-1,i}}\right] \tag{4}$$

where $d_{i-1,i}$, $\sigma_{i-1,i}$, and $l_{i-1,i}$ are the diameter, stress, and length of the fiber segment $(i-1, i)$, respectively. F_{Bi} is the surface tension force exerting on bead i, tends to restore the rectilinear shape of the bending part of the jet, and is given as

$$F_{Bi} = \frac{\alpha\pi\left(\frac{d_{i,i+1}+d_{i-1,i}}{2}\right)^2 k_i}{4(x_i^2 + y_i^2)^{1/2}}[\mathbf{i}x_i + \mathbf{j}y_i] \tag{5}$$

where α is the surface tension coefficient and k_i is the curvature of the jet segment $(i-1, i, i+1)$.

To model the way a spatial perturbation develops, an initial perturbation is added:

$$x_i = aL\sin(\omega t) \tag{6.a}$$

$$y_i = aL\cos(\omega t) \tag{6.b}$$

where x_i and y_i are the positions of bead i at x and y coordinates; ω is the perturbation frequency; a is a constant; and $L = (4e^2/\pi d_0^2 G)^{1/2}$ and is defined as the length scale, where d_0 is the initial jet diameter and G is the elastic modulus of the polymer solution.

When a is changed, the amplitude of the initial perturbation aL is changed. Therefore, when a and ω are changed during calculation, the effects of the amplitude and frequency of the initial perturbation on the development of whipping instability can be investigated. To characterize whipping motion, the amplitude of the whipping is introduced. *Whipping amplitude* is defined as the maximum lateral displacement at position z and is calculated as (x_{imax}^2

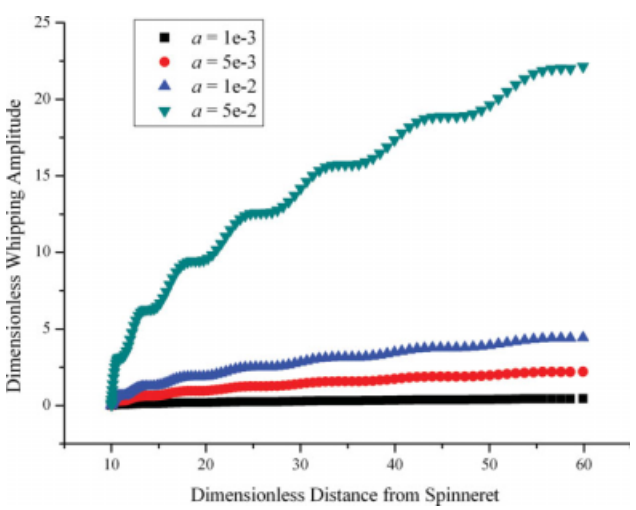

Figure 5 Effect of the amplitude of the initial perturbation on the whipping amplitude. [Color figure can be viewed in the online issue, which is available at www.interscience.wiley.com.]

$+ y_{imax}^2)^{1/2}$; where x_{imax} is the maximum displacement of x at position z and y_{imax} is the maximum displacement of y at position z. In this study, we changed a from 10^{-3} to 5×10^{-3} to 10^{-2} to 5×10^{-2} and changed ω from 10 to 50 by steps of 10. These parameters are dimensionless.

RESULTS AND DISCUSSION

Figure 5 shows the effect of the amplitude of the initial perturbation on the whipping amplitude. The calculations showed the whipping amplitude growth as the jet moved downward from the spinneret to the collector during the electrospinning process. For a $10^{-3}L$ initial perturbation amplitude, the whipping amplitude was very small. However, the whipping amplitude increased substantially as the amplitude of the initial perturbation increased.

Figure 6 shows the effect of the initial perturbation frequency on the whipping amplitude. The whipping amplitude decreased as the initial perturbation frequency increased. With increasing perturbation frequency, the period for the jet motion remained unvaried; whereas the whipping amplitude decreased, and the number of the loops of whipping increased.

Our experimental results show that a weaker perturbation under vacuum conditions led to a smaller S, which indicated a weaker whipping motion. Qualitative trends in the model predictions were in accordance with the experimental investigation.

The experimental results show that a weaker perturbation in the process caused slightly weaker whipping and slightly larger fiber diameters. Unfortunately, our modeling predictions showed that the amplitude and frequency of the initial perturbation had little influence on the fiber diameters. Figure 7 shows the effect of the perturbation frequency on the fiber diameter. In fact, it was not easy to obtain a realistic set of dimensionless perturbation amplitude and frequency for calculation. The discussion in this article is an initial exploration in this area, and we have focused on the effect of perturbations on the whipping motion for the first step of the study.

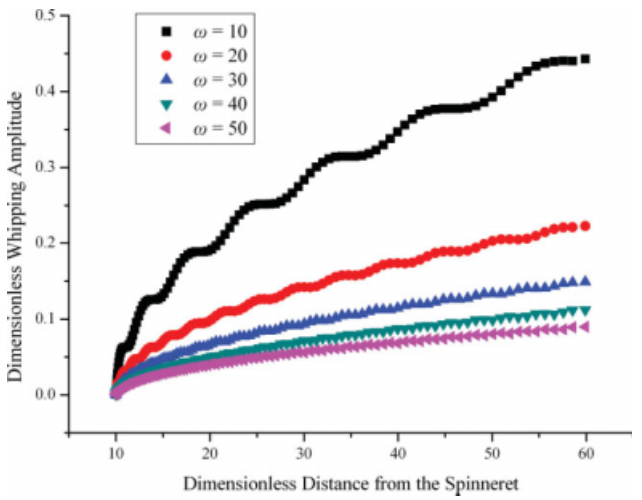

Figure 6 Effect of the initial perturbation frequency on the whipping amplitude. [Color figure can be viewed in the online issue, which is available at www.interscience.wiley.com.]

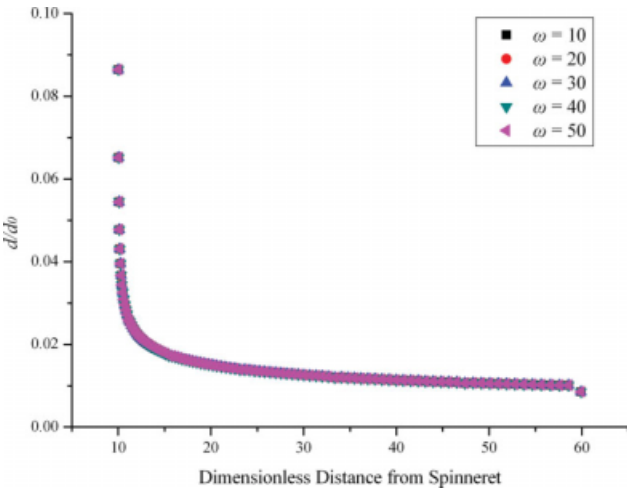

Figure 7 Effect of the initial perturbation frequency on the fiber diameter. [Color figure can be viewed in the online issue, which is available at www.interscience.wiley.com.]

CONCLUSIONS

The effect of perturbations on the whipping motion in electrospinning was studied with experimental and modeling methods. The experimental observations of electrospinning under normal and vacuum conditions showed that perturbations of ambient air influenced the whipping motion and the resulting fiber diameter to some extent. A weaker perturbation in the process caused slightly weaker whipping and slightly larger fiber diameters. An electrospinning model was adopted to predict the effect of initial perturbation on the whipping instability and the final fiber diameter. The predictions showed that the amplitude and frequency of the initial perturbation dramatically influenced the whipping amplitude. Qualitative trends in the model predictions were in accordance with the experimental investigation. However, the initial perturbation predicted little influence on the final fiber diameter.

The authors express their appreciation to W. Oxenham for his valuable discussion concerning this article.

References

1. Shin, Y. M.; Hohman, M. M.; Brenner, M. P.; Rutlege, G. C. Appl Phys Lett 2001, 78, 1149.
2. Shin, Y. M.; Hohman, M. M.; Brenner, M. P.; Rutlege, G. C. Polymer 2001, 42, 9955.

3. Hohman, M. M.; Shin, Y. M.; Rutledge, G. C.; Brenner, M. P. Phys Fluids 2001, 13, 2201.
4. Hohman, M. M.; Shin, Y. M.; Rutledge, G. C.; Brenner, M. P. Phys Fluids 2001, 13, 2221.
5. Reneker, D. H.; Yarin, A. L.; Fong, H.; Koombhongse, S. J Appl Phys 2000, 87, 4531.
6. Yarin, A. L.; Koombhongse, S.; Reneker, D. H. J Appl Phys 2001, 89, 3018.
7. Yarin, A. L.; Koombhongse, S.; Reneker, D. H. J Appl Phys 2001, 90, 4836.
8. Zeng, Y. C.; Wu, Y.; Pei, Z. G.; Yu, C. W. Int J Nonlinear Sci Numer Simul 2006, 7, 385.
9. Yang, Y.; Jia, Z. D.; Liu, J. N.; Li, Q.; Hou, L.; Wang, L. M.; Guan, Z. C. J Appl Phys 2008, 103, 104307.
10. Fridrikh, S. V.; Yu. J. H.; Brenner, M. P.; Rutledge, G. C. ACS Symp Ser 2006, 918, 36.